Transient CFD Simulation on Dynamic Characteristics of Annular Seal under Large Eccentricities and Disturbances

Kai Zhang [1], **Xinkuo Jiang** [2], **Shiyang Li** [1], **Bin Huang** [3], **Shuai Yang** [1], **Peng Wu** [1,*] **and Dazhuan Wu** [1,4]

1 College of Energy Engineering, Zhejiang University, Hangzhou 310027, China; zhangkai612@zju.edu.cn (K.Z.); lishiyang@zju.edu.cn (S.L.); shuaiyangzju@zju.edu.cn (S.Y.); wudazhuan@zju.edu.cn (D.W.)
2 China Tianchen Engineering Corporation, Tianjin 300400, China; jiangxinkuo@zju.edu.cn
3 Ocean College, Zhejiang University, Hangzhou 310027, China; binhuang@zju.edu.cn
4 State Key Laboratory of Fluid Power Transmission and Control, Hangzhou 310027, China
* Correspondence: roc@zju.edu.cn; Tel.: +86-1373-543-5349

check for updates

Abstract: Annular seals of turbomachinery usually suffer from various degrees of eccentricities and disturbances due to the rotor–stator misalignment and radial loads, while the discussion of annular seal under both large static eccentricities and dynamic disturbances is relatively limited. In this paper, the applicability of linear assumption and reliability of nonlinear dynamic model for eccentric annular seals under large eccentricities and disturbances is discussed based on the investigation of seals with various rotor motions through computational fluid dynamics (CFD). After the validation of transient CFD methods by comparison with experimental and bulk theory results, the dynamic behaviors of annular seal are analyzed by adopting both direct transient simulations and the nonlinear Muszynska model. The results show that the nonlinear dynamic model based on rotor circular whirls around seal center can predict the fluid excitations of different types of rotor motions well under small static eccentricities, while it is limited severely with large static eccentricities, which indicates that the dynamic characteristics of annular seal under large eccentricities are related with the rotor's motion ways. The paper provides a reference for studies of rotor–seal system with complex rotor motions considering radial loads or running across the resonance region.

Keywords: annular seal; CFD; dynamic coefficients; fluid forces; nonlinear dynamic model; static eccentricity

1. Introduction

Hydraulic machinery such as pumps and turbines is widely applied in various energy fields, playing a significant role in energy development, utilization and transformation. The vibration caused by the fluid forces generated in gap seals of hydraulic machinery tend to have important effects on the efficiency and vibration of rotor system [1]. Due to the rise of safety and efficiency concerns, dynamic characteristics of various annular seals have been studied by researchers [2–5]. Almost all of these studies are based on the assumption of small perturbation, hence linear dynamic characteristics of annular seals can be investigated. Generally, the annular seal is not the supporting element in design. Under the condition of static equilibrium, the rotor is normally concentric with the annular seal. Due to the axial-symmetry of seal geometry, as shown in Figure 1, the force coefficients of concentric seals show symmetric or skew symmetric features, as shown in Equation (1), where F_x, F_y are the X and Y components of fluid forces respectively; K and k denote direct and cross stiffness coefficients,

respectively; similarly, direct and cross damping coefficients are expressed as *C* and *c*, respectively; and *M* is direct mass coefficient. These five coefficients can be numerically computed by using the bulk flow model [6], CFD simulations by introducing moving reference frame [7,8] or transient method [9] and measured by perturbing the rotor or the stator [10].

$$-\left\{ \begin{array}{c} F_x \\ F_y \end{array} \right\} = \left[\begin{array}{cc} K & k \\ -k & K \end{array} \right] \left\{ \begin{array}{c} x \\ y \end{array} \right\} + \left[\begin{array}{cc} C & c \\ -c & C \end{array} \right] \left\{ \begin{array}{c} \dot{x} \\ \dot{y} \end{array} \right\} + \left[\begin{array}{cc} M & 0 \\ 0 & M \end{array} \right] \left\{ \begin{array}{c} \ddot{x} \\ \ddot{y} \end{array} \right\} \tag{1}$$
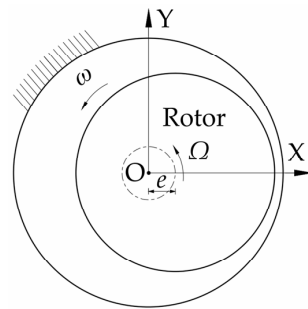

Figure 1. The circular whirl around seal center.

However, under actual condition, the static eccentricity of the rotor may exist in annular seal due to the misalignment during assembly process or the effects of various side loads (e.g., impeller weight). The dynamic characteristics of eccentric annular seals, as shown in Figure 2, were also investigated based on the bulk flow model by Nelson and Nguyen [11]. The fluid force increments (ΔF_x and ΔF_y) induced by the small perturbation around static eccentricity position are similarly expressed in linearized rotordynamic form, as shown in Equation (2) [12].

$$-\left\{ \begin{array}{c} \Delta F_x \\ \Delta F_y \end{array} \right\} = \left[\begin{array}{cc} k_{xx} & k_{xy} \\ k_{yx} & k_{yy} \end{array} \right] \left\{ \begin{array}{c} \Delta x \\ \Delta y \end{array} \right\} + \left[\begin{array}{cc} c_{xx} & c_{xy} \\ c_{yx} & c_{yy} \end{array} \right] \left\{ \begin{array}{c} \Delta \dot{x} \\ \Delta \dot{y} \end{array} \right\} + \left[\begin{array}{cc} m_{xx} & 0 \\ 0 & m_{yy} \end{array} \right] \left\{ \begin{array}{c} \Delta \ddot{x} \\ \Delta \ddot{y} \end{array} \right\}, \tag{2}$$

where Δx and Δy define the rotor motion relative to the equilibrium position. Unlike concentric seals, the force coefficients of eccentric seals are no longer symmetric or skew symmetric due to rotor misalignment. This brings difficulties to the numerical solutions of force coefficients. Arghir and Frene [13] compared the bulk flow model of concentric seals and eccentric seals, the results showing that the terms of circumferential partial derivatives emerge in all bulk flow equations due to the static eccentricity of flow field. This can result in the coupling effect between circumferential momentum equation and continuity equation and make the solutions of both bulk flow equations and their perturbation equations very complex. As to the CFD method, the seal flow field disturbed by rotor circular whirl is not axisymmetric, as shown in Figure 2, and the steady-state simplified treatment by introducing moving reference frame is no longer applicable [8]. This means that transient simulations are necessary for evaluating force coefficients of eccentric seals.
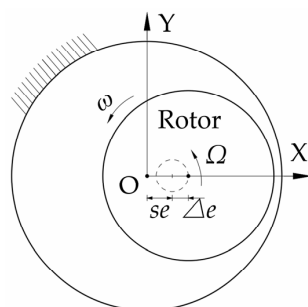

Figure 2. The circular whirl around equilibrium position.

To overcome numerical difficulties in eccentric seal research, Venkataraman and Palazzolo [14] determined the circumferential derivatives through a cubic spline interpolation method and simplified the bulk flow equations of eccentric seals. Athavale and Hendricks [15] presented a small perturbation CFD method for calculation of rotordynamic coefficients of concentric and eccentric seals, and the SCISEAL code along with a modified SIMPLEC algorithm was adopted. Wu et al. [16] developed a new transient CFD method, which is based on rotor's variable-speed whirl; the results show that this new method can keep good accuracy of traditional transient method and save much computational time and cost in the meantime.

The research for fluid force presented above has mainly focused on linear fluid force analysis, and it was performed under the strict restriction and assumption that the whirl amplitude is relatively very small compared to the seal clearance (within 0.1 C_r; C_r denotes the seal clearance). While large amplitude vibration often occurs during the passage of the critical speed of actual turbomachinery, the linear bulk flow analysis may not be applicable for the accurate fluid force characteristics in such situations with large amplitude. To describe the fluid forces of annular seal induced by large disturbances, the nonlinear dynamic model should be established. San Andres and Jeung [17] presented an orbit analysis method based on extended Reynolds equation to investigate force coefficients valid over a wide frequency range of a squeeze film damper bearing with large amplitude and static eccentricity. Ikemoto et al. [6] investigated the nonlinear fluid forces for the concentric seal with large whirl amplitude up to about a half of the clearance by using extended perturbation analysis of the bulk flow theory. Currently, the Muszynska's model proposed by Bently and Muszynska [18] is commonly used by researchers as a nonlinear dynamic model. Li and Chen [19] adopted the Muszynska's seal force model with the empirical parameters to investigate the 1:2 subharmonic resonance of labyrinth seal–rotor system. These empirical parameters obtained by employing the CFD analysis are used in the subsequent nonlinear analysis, regardless of whether the whirl amplitude is around the concentric position or not. He and Jing [20] indicated that Muszynska's model will not describe the dynamic characteristics of the rotor–seal system well when the rotor–seal system has larger eccentricity ratio. However, the present paper is devoted to develop nonlinear dynamic models of concentric seal with large whirl amplitude or eccentric seal with large static eccentricity and rather small whirl amplitude. The applicability of linear assumption and reliability of nonlinear model for seals under large static eccentricities and disturbance amplitude is rarely discussed in the literature. Thus, an investigation on the applicability of nonlinear Muszynska's model under large eccentricities and disturbances is wished for, particularly in nonlinear rotor–seal system research considering radial loads.

In experimental studies of eccentric seals, Marquette, Childs and Andres [21] measured the force coefficients of a plain liquid annular seal under different static eccentricities, and the results show that the force coefficients were more sensitive to the changes of static eccentricity than theoretically predicted. Childs, Arthur and Mehta [22] measured the net reaction forces of gas annular seals as the eccentricity ratios increased; negative stiffness created by unanticipated eccentricities may lead to over prediction of critical speeds, which illustrates the importance of concentric assembly of annular seals.

In this paper, three-dimensional (3D) transient CFD simulations based on dynamic mesh method are performed to evaluate the static and dynamic characteristics of eccentric annular seals. The obtained force coefficients and leakage rates are compared with Marquette's experiment [21] for validating the reliability of the transient CFD method. The effects of rotor disturbance amplitude on the dynamic characteristics of eccentric annular seals are analyzed to investigate the linear ranges of seal dynamic characteristics. In addition, transient CFD simulations and a nonlinear dynamic model are adopted to study the fluid excitations of annular seals induced by different rotor large motions. The nonlinear dynamic model is based on the famous Muszynska's model [18,23,24] and is obtained by fitting the "nominal" force coefficients of concentric annular seal under different whirl amplitude, as shown in Figure 2. With nonlinear model and transient CFD simulations, fluid excitations under various large disturbances are computed. Based on these fluid excitations, seal dynamic characteristics under large

eccentricities and disturbances are investigated in detail, which provides a solid basis for the research of seal–rotor system analysis by using Muszynska' model as nonlinear seal force.

2. Numerical Methods

2.1. Geometry Model and Grid

The plain annular seal adopted to perform the studies in this paper is applied in high speed hydrostatic journal bearings, which is tested in the apparatus and facility in Marquette's experiment. The work medium is water at 20 °C. The geometric and operating parameters of the seal are listed in Table 1. As shown in Figure 3, the structured grids are generated in the concentric annular fluid domain by the CFD Preprocessor Gambit, which is geometry and mesh generation commercial software for computational fluid dynamics (CFD) analysis.

Table 1. Parameters of plain annular seal.

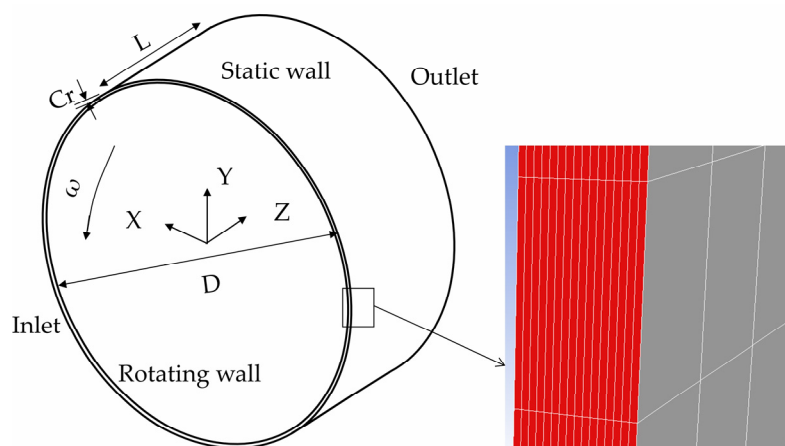| Main Parameters	Symbols	Values	Units
seal length	L	34.93	mm
seal diameter	D	76.29	mm
seal clearance	C_r	0.11	mm
rotating speed	ω		rpm
pressure difference	ΔP	5.52	MPa
length-diameter ratio	L/D	0.46	

Figure 3. Numerical model of concentric annular seal.

The grid independence is checked by comparing the several grids with different radial grid densities. Under 80% eccentricity ratio, the radial and tangential components of fluid force are evaluated according to different grid models, as shown in Figure 4. The curves of "Fr refined" and "Ft refined" represent the radial and tangential fluid force of refined grid model, which has 36 radial layers with more than 10 layers near the both walls to keep y+ less than 5. The grid model of 16 radial layers is adopted considering the accuracy and computational time. With respect to the tangential and axial density, it can be seen in Table 2 that the results of fluid force show good convergence at Grid 3 ($16 \times 318 \times 1448$, i.e., there are 16 layers of grids generated along seal clearance in radial direction, 318 layers in axial direction and 1448 layers in circumferential direction) as the grid density changes to 1.25 or 1.5 times. This indicates that the present grid resolution ($16 \times 318 \times 1448$, 7,358,770 grid cells) is suitable for this research considering about the accuracy and efficiency of simulations.
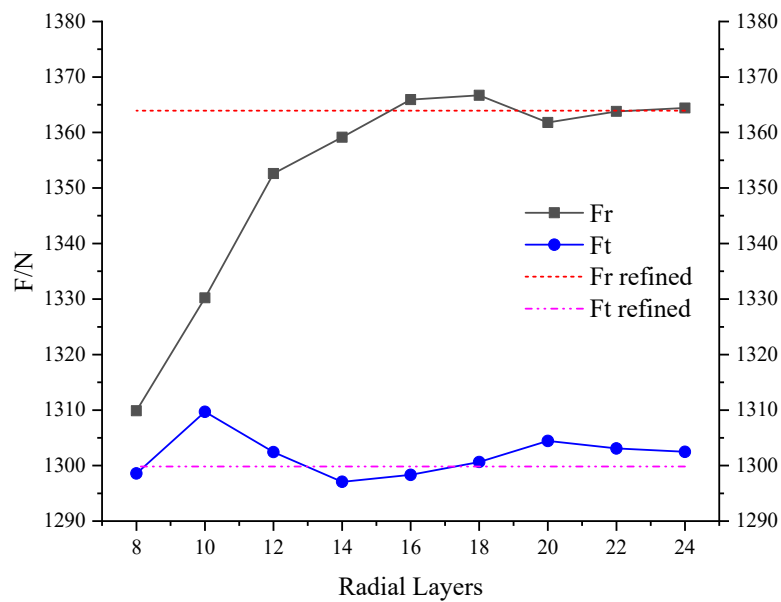
Figure 4. Radial grid density study.

Table 2. Tangential and axial grid density study.

Name	Grid Density	Fr/N	Relative Error [1]	Ft/N	Relative Error [1]
Grid 1	$16 \times 204 \times 1448$	1331.43	2.53%	1278.62	1.52%
Grid 2	$16 \times 254 \times 1448$	1358.79	0.52%	1289.26	0.70%
Grid 3	$16 \times 318 \times 1448$	1365.92	-	1298.33	-
Grid 4	$16 \times 397 \times 1448$	1367.51	−0.12%	1299.54	−0.09%
Grid 5	$16 \times 477 \times 1448$	1367.86	−0.14%	1300.15	−0.14%
Grid 6	$16 \times 318 \times 926$	1344.51	1.57%	1276.36	1.69%
Grid 7	$16 \times 318 \times 1158$	1360.28	0.41%	1290.79	0.58%
Grid 8	$16 \times 318 \times 1810$	1366.09	−0.01%	1298.65	−0.02%
Grid 9	$16 \times 318 \times 2170$	1365.82	0.01%	1298.93	−0.05%

[1] Note: by comparing with Grid 3 ($16 \times 318 \times 1448$, radial × axial × tangential layers).

2.2. 3D Transient Solutions

Under various rotor disturbances, the static and dynamic characteristics of plain annular seal are investigated by simulating the transient flow in seal clearance. In this paper, the commercial CFD solver, ANSYS Fluent, is chosen to solve the 3D Reynolds-averaged Navier–Stokes equations. To achieve transient simulations, dynamic mesh problem should be firstly settled. As shown in Figure 2, the motion of rotor (i.e., rotating wall) can change the shape of fluid domain, and grids will change accordingly. However, due to high aspect ratio of grid cells in the clearance, the three types of dynamic methods in Fluent—spring-based smoothing, local remeshing and dynamic layering methods—tend to cause bad orthogonality or negative volume of grids.

To ensure good grid quality, the dynamic mesh model based on interpolation method [9,25] is adopted in this paper, which can effectively control the movement of the girds. First, nodes on rotating wall (i.e., rotor surface) are controlled to move according to the motion equation of the rotor and nodes on static wall keep stationary. Then, the ratio of nodes in the clearance is deduced according to the geometric relations of position of nodes in the clearance and movement of rotor. After that, the motions of grid nodes in the domain are determined by using the interpolation method based on the distances of the nodes from rotor and stator walls. Finally, the positions and velocities of grid nodes in the domain are obtained after the movement of rotor.

Figure 5 shows the grid nodes moving in the clearance of annular seal. As illustrated in the figure, pf^0 (x^0_f, y^0_f) and pb^0 (x^0_b, y^0_b) represent the nodes of rotor surface and stator surface, respectively,

when the rotor is at the concentric position. pi^0 (x^0_i, y^0_i) is an arbitrary node in the clearance domain of annular seal along the line between pf^0 and pb^0. θ denotes the initial angular coordinate of node pf^0. The superscript denotes the moving step of nodes and the subscript denotes the position of nodes. $d^1(x^1_d, y^1_d)$ represents the motion vector of moving rotor in Cartesian coordinates. di^1 denotes the vector from pi^0 to pi^1 (x^1_i, y^1_i). Then, the new coordinates (x^1_f, y^1_f) of pf^0 (current node pf^1) are defined as Equation (3).

$$x^1_f = x^0_f + x^1_d, \ y^1_f = y^0_f + y^1_d,$$ (3)
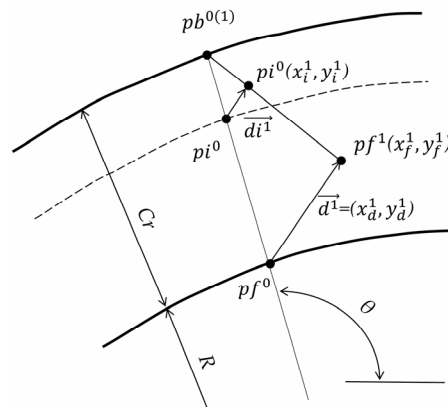
Figure 5. Schematic diagram of moving grid node.

The node of stator surface is assumed to stay still, the movement distance between rotor and stator is determined by the interpolation algorithm. Then, the new position coordinates (x^1_f, y^1_f) of pi^1 could be expressed as Equation (4).

$$x^1_i = x^0_i + ra \times x^1_d, \ y^1_i = y^0_i + ra \times y^1_d,$$ (4)

where ra denotes the ratio of the distance between the nodes in the clearance domain and the static outer wall to the clearance. When the rotor is in concentric and eccentric position, the initial angular coordinate θ of pf^0 and the ratio of ra can be expressed by known parameters R and C_r and the coordinates of pf^0, pi^0 and pb^0 according to collinear geometric relations of pf^1, pi^1 and pb^1. Then, the new position of pi^1 in the clearance after the movement of rotor can be obtained by substituting ra to Equation (3).

The displacement of each node is restricted and calculated by mathematical procedures, which strictly ensures the movement coordination of adjacent grid nodes. The whole dynamic mesh process is implemented by adopting a subroutine linked with the CFD solver. This algorithm has been tested and the results show that, when the rotor whirled from the concentric position (with exaggerated seal clearance C_r), as shown in Figure 6a, to the eccentric position, as shown in Figure 6b, the grid distortion rate will increase but there is no negative volumes and highly distorted elements. The maximum grid aspect ratio will not exceed 200 even with eccentricity ratios (e/C_r, e denotes the rotor eccentricity) of 80%, which indicates that this dynamic mesh algorithm is suitable for the transient simulation with large eccentricity.

Due to rotor eccentricity, one side of the grids is compressed and the maximum aspect ratio of the grids increases on basis of the initial grid model in Figure 6a. Considering the extreme thin grid layers, numerical computations are performed under double precision to ensure the stability and reliability of the result. The boundary conditions of 5.52 MPa total pressure and 0 Pa static pressure are, respectively, adopted at inlet and outlet. Both walls are set as no-slip walls and the rotating wall possesses a rotation speed which equals to r/min. The wall y+ of flow field under various disturbances is generally located in the range of 20–40 and the Realizable k-ε model with enhanced wall function is suitable to handle the

situation [9,16]. The first-order implicit scheme is used for the discretization of time term. The chosen time step is equal to the wall rotation for 1 degree so that the courant number in most regions can be confined within 5 for stability. More than 360 steps are performed to ensure the stability of transient simulation according to different rotor motions. The second-order up-wind scheme with numerical under-relaxation is adopted to the convection term in the equations. The central-differencing scheme is employed to discretize the diffusion. The velocity–pressure coupling is solved by using the well-known SIMPLE strategy. Each simulation case for one revolution costs about 50 h on the platform of CPU is Intel® Xeon® Gold 6240 @ 2.60GHz with an average 16-parallel-processes solver.

(a)   **(b)**
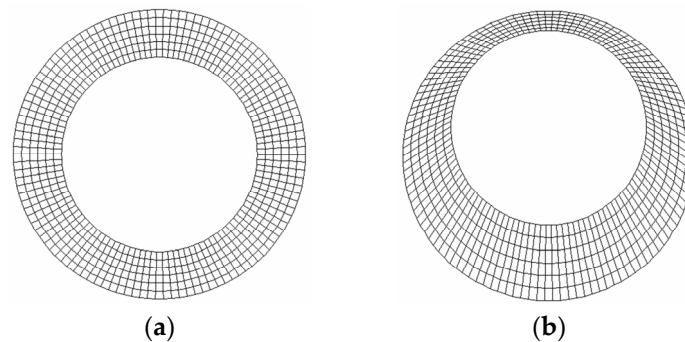
Figure 6. Diagram of cross section of the meshed rotor: (**a**) initial grids; and (**b**) moved grids.

2.3. Computing Static and Dynamic Characteristics of Eccentric Annular Seals

Transient CFD simulations are used to compute the static and dynamic characteristics of eccentric seals. The six cases with different static eccentricity ratios (se/C_r, where se denotes the static eccentricity of rotor) are investigated, respectively, 0%, 10%, 20%, 30%, 40% and 50%. The eccentric direction in +X direction is shown in Figure 2. The leakage rates of eccentric annular seals can be obtained by simulating the steady-state flow fields without rotor disturbances. The dynamic characteristics of eccentric seals can be analyzed by considering small rotor perturbations. The adopted perturbation is the circular whirl with a small whirl amplitude Δe (termed as dynamic eccentricity), as shown in Figure 2. The whirling speed Ω is constant. Given the suitability of small perturbation assumption, dynamic eccentricity ratio ($\Delta e/C_r$) should be very small (1% in the study). The small whirls are described by Equation (5). The fluid force increments (ΔF_x and ΔF_y) induced by perturbations are expressed by Equation (6).

$$\begin{cases} \Delta x = x - se = \Delta e cos(\Omega t) \\ \Delta y = y - 0 = \Delta e sin(\Omega t) \end{cases}, \tag{5}$$

$$\begin{cases} \Delta F_x = F_x - F_{x0} \\ \Delta F_y = F_y - F_{y0} \end{cases}, \tag{6}$$

where F_{x0} and F_{y0} represent fluid forces at equilibrium position. Substituting Equations (5) and (6) into Equation (2), F_x and F_y can be expressed as the harmonic functions of time, as shown in Equation (7):

$$\begin{cases} F_x = F_{x0} + A_1 \Delta e cos(\Omega t) + B_1 \Delta e sin(\Omega t) \\ F_y = F_{y0} + B_2 \Delta e cos(\Omega t) + A_2 \Delta e sin(\Omega t) \end{cases}, \tag{7}$$

where

$$\begin{cases} A_1 = -k_{xx} - c_{xy}\Omega + m_{xx}\Omega^2 \\ B_1 = -k_{xy} + c_{xx}\Omega + m_{xy}\Omega^2 \\ A_2 = -k_{yy} + c_{yx}\Omega + m_{yy}\Omega^2 \\ B_2 = -k_{yx} - c_{yy}\Omega + m_{yx}\Omega^2 \end{cases} \tag{8}$$

By simulating the transient flow field with rotor perturbation, the time histories of F_x and F_y can be recorded by integrating the fluid pressure at each time step. Then, they are used to evaluate F_{x0},

F_{y0} and the four constant coefficients (A_1, B_1, A_2 and B_2) in Equation (7) by curve fittings. A_1, B_1, A_2 and B_2 are composed of a known whirling speed Ω and three unknown force coefficients, as shown in Equation (8). To obtain all the unknown force coefficients, A_1, B_1, A_2 and B_2 under at least three (generally five is desired considering the fitting error) whirling speeds should be determined. Hence, at least three transient CFD simulations should be performed.

2.4. Fitting Nonlinear Dynamic Model

Force coefficients of annular seals can only be used to describe fluid forces induced by rotor small perturbations. The Muszynska's model is adopted to describe the fluid forces of annular seal induced by large disturbances. It is derived based on a serial of experiments and adopts nonlinear dynamic parameters similar with force coefficients to associate fluid forces with rotor motion, as shown in Equation (9):

$$\left\{ \begin{matrix} F_x \\ F_y \end{matrix} \right\} = - \left[\begin{matrix} S - m_f \tau_1^2 \omega^2 & \tau_1 \omega D \\ -\tau_1 \omega D & S - m_f \tau_1^2 \omega^2 \end{matrix} \right] \left\{ \begin{matrix} x \\ y \end{matrix} \right\} - \left[\begin{matrix} D & 2\tau_1 \omega m_f \\ -2\tau_1 \omega m_f & D \end{matrix} \right] \left\{ \begin{matrix} \dot{x} \\ \dot{y} \end{matrix} \right\} - \left[\begin{matrix} m_f & 0 \\ 0 & m_f \end{matrix} \right] \left\{ \begin{matrix} \ddot{x} \\ \ddot{y} \end{matrix} \right\}, \quad (9)$$

where $S = S_0 \left(1 - \varepsilon^2\right)^{-n}$, $\tau_1 = \tau_0 (1 - \varepsilon)^b$, $D = D_0 \left(1 - \varepsilon^2\right)^{-n}$, for $\varepsilon = \sqrt{x^2 + y^2}/C_r$

n, τ_0 and b are empirical factors for certain seal structure; S_0, D_0 and m_f can be computed using Black–Childs formulas [26]. When the seal is under steady working condition (constant ω and ΔP), the S_0, D_0, m_f and empirical factors in Muszynska's model become constant values. Namely, nonlinear dynamic parameters in matrices are only related with eccentricity ratio ε. Thus, Equation (9) can be expressed in a simplified form, as shown in Equation (10):

$$\left\{ \begin{matrix} F_x \\ F_y \end{matrix} \right\} = - \left[\begin{matrix} K(\varepsilon) & k(\varepsilon) \\ -k(\varepsilon) & K(\varepsilon) \end{matrix} \right] \left\{ \begin{matrix} x \\ y \end{matrix} \right\} - \left[\begin{matrix} C(\varepsilon) & c(\varepsilon) \\ -c(\varepsilon) & C(\varepsilon) \end{matrix} \right] \left\{ \begin{matrix} \dot{x} \\ \dot{y} \end{matrix} \right\} - \left[\begin{matrix} M(\varepsilon) & 0 \\ 0 & M(\varepsilon) \end{matrix} \right] \left\{ \begin{matrix} \ddot{x} \\ \ddot{y} \end{matrix} \right\}, \quad (10)$$

The Muszynska's model under constant working condition is very similar to the linear dynamic model of concentric annular seal in Equation (1). The only difference is that dynamic parameters in Equation (10) are nonlinear functions of ε and can be used to describe fluid forces induced by rotor large disturbances. The expressions of nonlinear dynamic parameters can be determined based on the formulas in Equation (9), but proper empirical factors need to be chosen. In addition, the nonlinear expressions can be fitted based on the "nominal" force coefficients of concentric seal under different eccentricities (as shown in Figure 2). These "nominal" force coefficients can be computed by using CFD methods [8,27]. Rotor perturbation is the circular whirl around seal center. Usually, whirl amplitude (i.e., rotor eccentricity) is controlled within $0.1C_r$ for satisfying the linear assumption. To obtain "nominal" force coefficients under different eccentricities, the limitation is broken here, and the adopted whirl amplitudes are located in the range of $0.01C_r$–$0.8C_r$ (i.e., ε in 1%–80%).

Transient CFD simulations are conducted to solve the flow field disturbed by constant-speed circular whirls, and fluid-induced forces can be obtained. Based on these fluid forces, the "nominal" force coefficients of concentric annular seal can be evaluated [8] and used to generate the nonlinear dynamic model. With respect to the Muszynska's model, the new nonlinear model does not need any empirical factors. Theoretically, it can describe fluid forces (seal forces) induced by various rotor motions within eccentricity ratio 80%. Its reliability and suitability are discussed in Section 3.

3. Results and Discussions

3.1. Dynamic Characteristics of Different Static Eccentric Seals and Comparisons

The leakage rates and force coefficients of annular seal under different static eccentricity positions and same whirl amplitude ratio ($\Delta e/C_r = 1\%$) are computed using the numerical scheme based on transient CFD simulations (see Section 2.3). They are, respectively, shown in Figures 7–12 along with the results from San Andres' bulk flow method and Marquette's experiments.
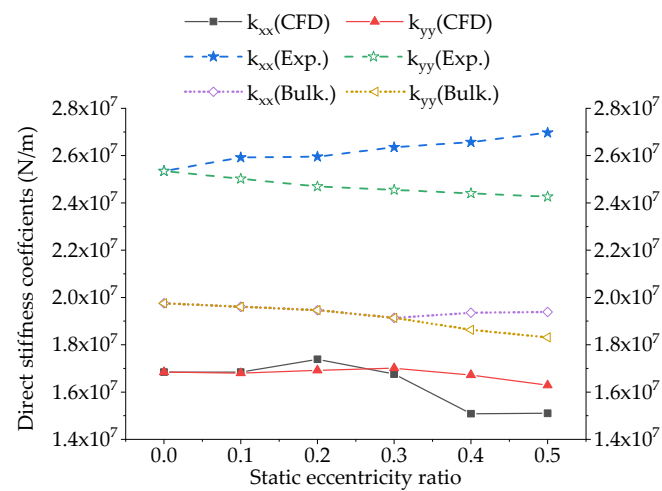
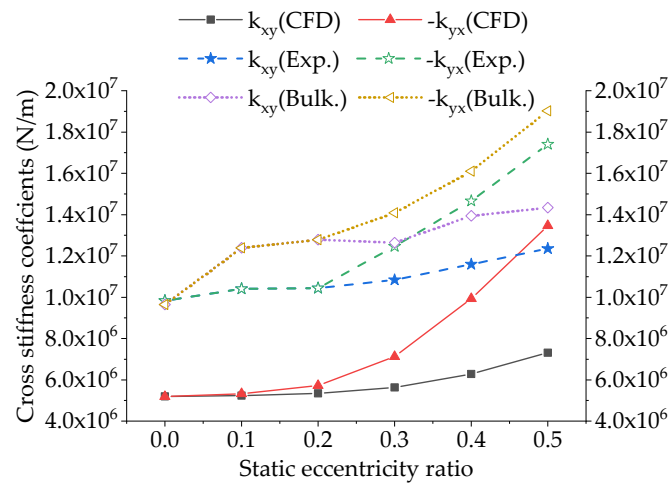**Figure 7.** Direct Stiffness coefficients of eccentric annular seals.

Figure 8. Cross Stiffness coefficients of eccentric annular seals.
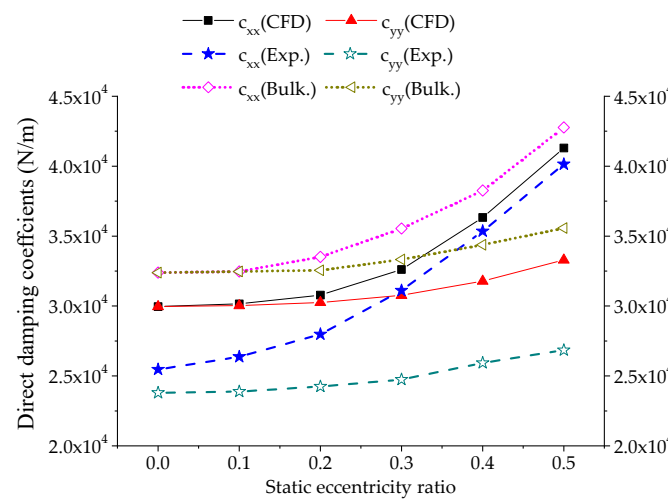

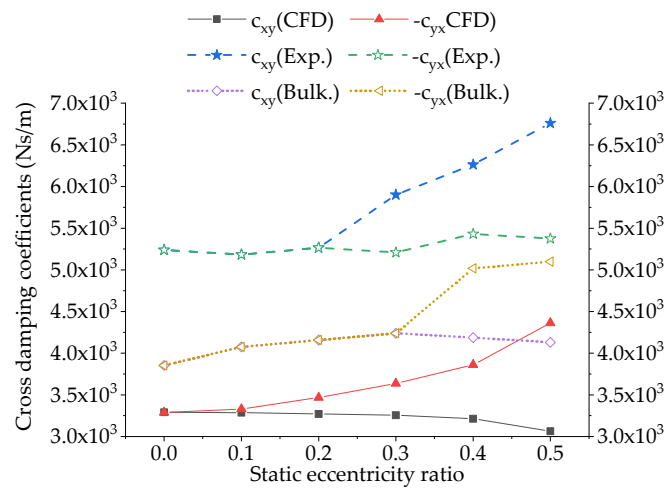**Figure 9.** Direct damping coefficients of eccentric annular seals.

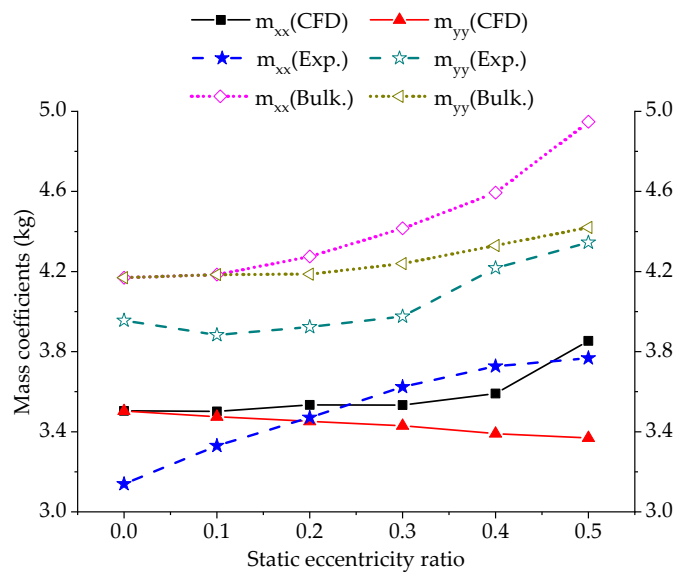**Figure 10.** Cross damping coefficients of eccentric annular seals.

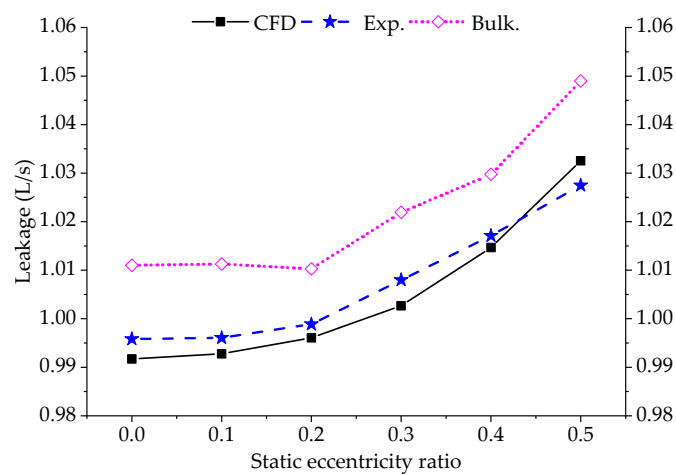**Figure 11.** Mass coefficients of eccentric annular seals.

Figure 12. Leakage rates of eccentric annular seals.

In Figures 7 and 8, the measured values of direct and cross stiffness coefficients are larger than numerical values from transient CFD simulations. The test apparatus of Marquette's experiment does not include any device to control or measure the inlet swirl, and the non-uniformity of incoming flow is not considered during the testing procedure, which may lead to variations of stiffness coefficients with eccentric directions according to Wu's research [28]. The boundary condition of seal model illustrated in Marquette's research is only pressure condition for inlet and outlet. There is no geometry information or measurement of inlet, which is also mentioned by the authors as a drawback. The reason of the lower accuracy is that it is much difficult to ensure the boundary condition of CFD analysis, especially for the inlet, consistent with the Marquette's experiment. Tae Woong Ha's study [27] shows the similar difference between the stiffness results of CFD analysis and the experimental results. Despite the differences of values in Figure 7, it shows a high level of consistency between results of transient simulations and measured values as static eccentricity ratio increases.

In Figures 9 and 10, direct damping coefficients from transient simulations and bulk flow method are both a little higher than measured values, and CFD results are closer to experimental values. Cross damping coefficients from the three approaches are all close in size. As shown in Figure 11, although numerical results of mass coefficients do not coincide with measured values in variation trend, they are close in size.

Figure 12 shows the variations of seal leakage rate with the eccentricity. As rotor eccentricity increases, seal leakage rate just slightly rises. In Figure 12, leakage rates computed by transient simulations are very close to measured values, which further indicate the reliability of CFD method. This also shows that leakage rates of annular seals mainly depend on sealed differential pressures and are not sensitive to flow status at seal inlet, unlike force coefficients [28].

On the whole, rotor eccentricities change the static and dynamic characteristics of annular seals to some extent; the behaviors of annular seals should be specially considered when the rotor is far away from seal center. By comparing with experimental data, transient CFD simulations are effective in computing the static and dynamic behaviors of eccentric seals.

3.2. Effects of Disturbance Amplitude on Force Coefficients of Eccentric Annular Seal

The force coefficients of eccentric seals in Figures 7–12 are computed using a very small dynamic eccentricity (eccentricity ratio 1%). To study the effects of disturbance amplitude, two more dynamic eccentricity ratios, 5% and 10%, are separately adopted to evaluate force coefficients of eccentric seals. The results are presented in Figures 13–17 for comparisons.
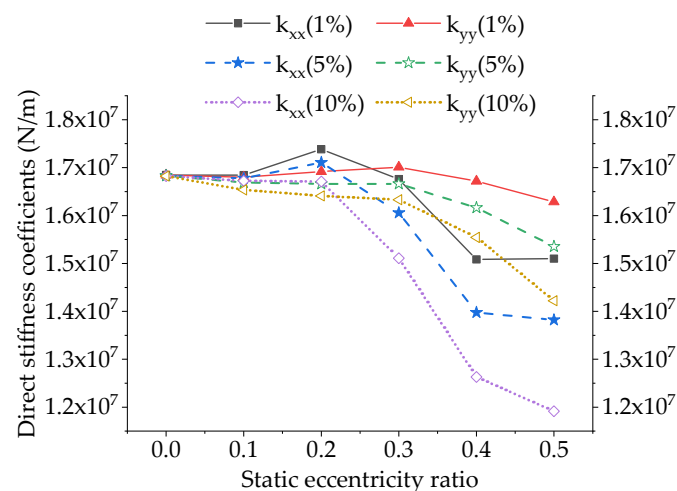

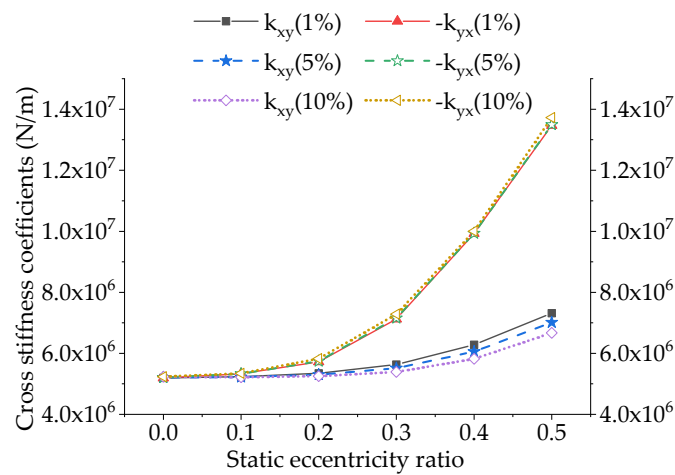**Figure 13.** Direct stiffness coefficients under different dynamic eccentricities.

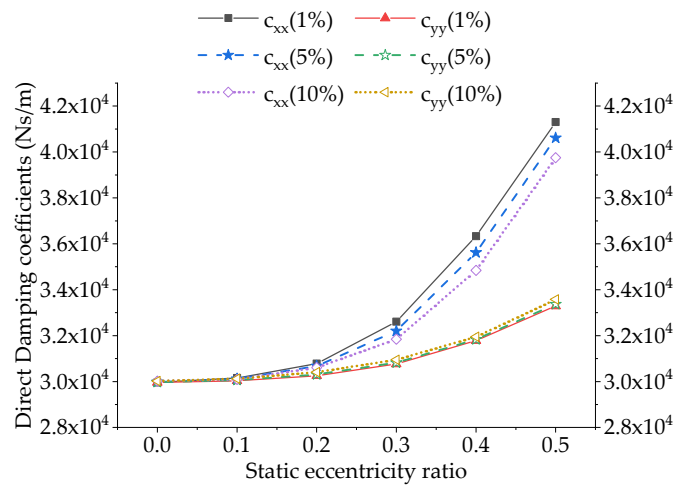**Figure 14.** Cross stiffness coefficients under different dynamic eccentricities.

Figure 15. Direct damping coefficients under different dynamic eccentricities.
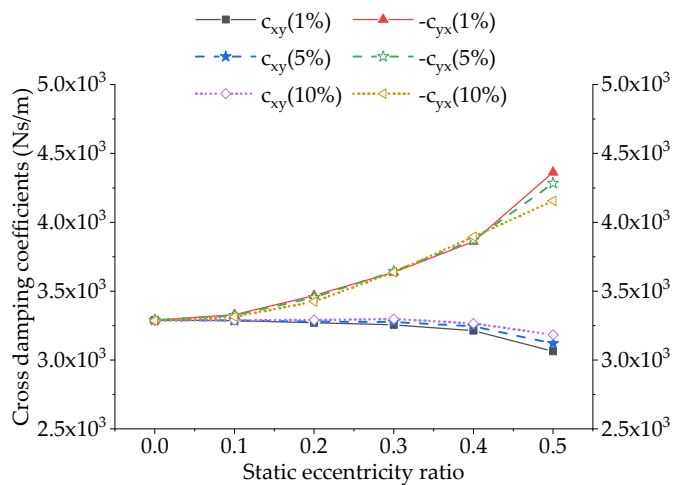

Figure 16. Cross damping coefficients under different dynamic eccentricities.
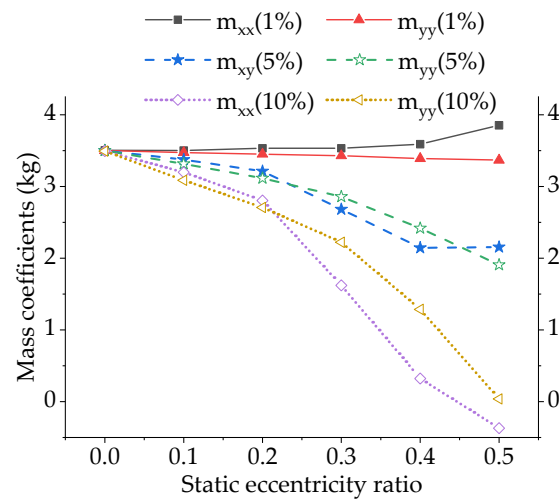
Figure 17. Mass coefficients under different dynamic eccentricities.

As shown in Figures 13–17, force coefficients based on three dynamic eccentricities are not the same. Their differences grow gradually as rotor static eccentricity increases, especially the coefficients k_{xx}, k_{yy}, k_{xy}, c_{xx}, m_{xx} and m_{yy}. For the concentric seal with static eccentricity zero, its force coefficients are generally unchanged with varying dynamic eccentricities. Namely, the dynamic characteristics of concentric annular seal are still linear when dynamic eccentricity ratio reaches 10%, which has been widely recognized by researchers [7,8,29]. However, as to the eccentric annular seal, its force coefficients tend to be sensitive to dynamic eccentricities (i.e., disturbance amplitude). As rotor static eccentricity increases, the sensitivity to rotor disturbances strengthens gradually and the linear range of seal dynamic characteristics narrows. With respect to the concentric seal, the annular seal under large eccentricity is more likely to show nonlinear characteristics.

3.3. Nonlinear Dynamic Model

As discussed above, force coefficients of eccentric seals can only be used to describe fluid forces induced by very small perturbations due to their strong sensitivity to disturbance amplitude. To express seal forces under large eccentricities or large disturbances, the nonlinear dynamic model is determined based on the thought in Section 2.3. The "nominal" force coefficients of concentric seal are computed based on different whirl amplitudes. They are presented in Figure 18 along with polynomial fitting curves. Piecewise fittings are used for direct stiffness *K* and cross damping *c*. As shown in Figure 18, the fitting effects of five force coefficients are satisfactory. The nonlinear expressions of these coefficients are listed as follows:

$$K(\varepsilon)\left(\times 10^6\right) = \begin{cases} 2.71\varepsilon^2 - 0.703\varepsilon + 16.9, & \varepsilon \leq 0.1, R^2 = 1 \\ 1.70\varepsilon^3 - 8.67\varepsilon^2 + 4.21\varepsilon + 16.5, & 0.1 < \varepsilon \leq 0.8, R^2 = 0.9911 \end{cases} \tag{11}$$

$$c(\varepsilon)\left(\times 10^3\right) = \begin{cases} -16.2\varepsilon^4 + 10.8\varepsilon^3 - 2.20\varepsilon^2 + 0.0767\varepsilon + 3.29, & \varepsilon \leq 0.4, R^2 = 0.9995 \\ -2.28 + 6.15\varepsilon^2 - 5.43\varepsilon + 4.58, & 0.4 < \varepsilon \leq 0.8, R^2 = 0.9997 \end{cases} \tag{12}$$

$$M(\varepsilon) = -5.28\varepsilon^4 + 6.63\varepsilon^3 - 3.58\varepsilon^2 + 0.36\varepsilon + 3.50, \quad \varepsilon \leq 0.8, R^2 = 0.9905 \tag{13}$$

$$k(\varepsilon)\left(\times 10^7\right) = 14.5\varepsilon^5 - 24.2\varepsilon^4 + 15.5\varepsilon^3 - 3.22\varepsilon^2 + 0.250\varepsilon + 0.517, \quad \varepsilon \leq 0.8$$
$$R^2 = 0.9999 \tag{14}$$

$$C(\varepsilon)\left(\times 10^4\right) = 10.7\varepsilon^4 - 11.6\varepsilon^3 + 5.57\varepsilon^2 - 0.682\varepsilon + 3.01, \quad \varepsilon \leq 0.8, R^2 = 0.9994 \tag{15}$$
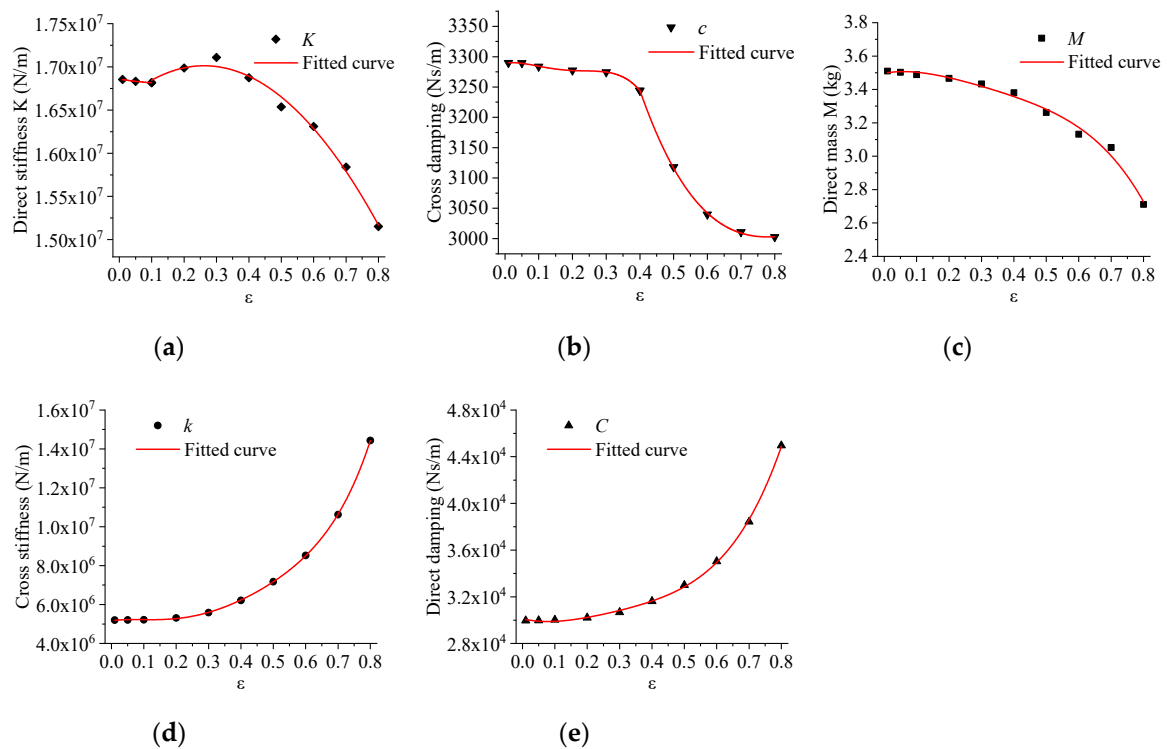
Figure 18. "Nominal" force coefficients of concentric annular seal: (**a**) direct stiffness; (**b**) cross damping; (**c**) direct mass; (**d**) cross stiffness; and (**e**) direct damping.

Substituting these nonlinear expressions into Equation (10), the nonlinear dynamic model is obtained. It will be used to evaluate fluid forces induced by rotor large disturbances along with transient CFD simulations.

4. Fluid Excitations under Large Disturbances

The fluid forces of annular seal under rotor large motions are computed by nonlinear dynamic model as well as transient CFD simulations. The suitability of nonlinear dynamic model for various rotor disturbances is investigated through comparisons with direct transient simulations. Several typical rotor motions are chosen for the investigation.

4.1. Constant-Speed Circular Whirl Around Seal Center

The rotor performs circular whirl around seal center with speed 10,200 r/min (Figure 1) and the whirl magnitude is 55% C_r. The motion equation is shown as below. Substituting Equations (11)–(16) into Equation (10), the induced fluid forces (F_x and F_y) are obtained by the nonlinear dynamic model. They are shown in Figure 19 along with the results from transient CFD simulations.

$$\begin{cases} x = ecos(\Omega t) \\ y = esin(\Omega t) \end{cases} \tag{16}$$

Because the prescribed initial solution is not absolutely accurate, the transient CFD computation needs passing a period of time to eliminate its effects. Fluid forces computed at initial some time steps are not true and can be ignored. In Figure 19, fluid force curves from nonlinear dynamic model and transient CFD simulations are in good agreement. Maximum differences are only 16.5 N for both F_x and F_y, and they are mainly caused by fitting and computing errors. This indicates that the present nonlinear dynamic model is adequate to describe seal fluid excitations induced by circular whirls around seal center.
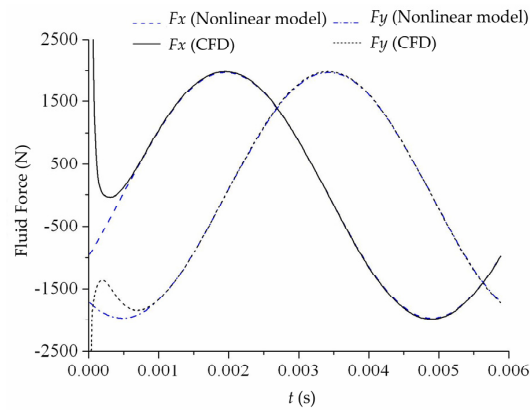
Figure 19. Fluid forces induced by the circular whirl around seal center.

4.2. Constant-Speed Circular Whirl Around Static Position

The rotor is assumed to perform circular whirl around static eccentricity position, as shown in Figure 2. The dynamic eccentricity ratio is 10%. Two whirl centers correspond to static eccentricity ratio 20% and 50%, respectively. The whirling speed is same with the rotating speed, 10,200 r/min. Rotor movements (x, y) can be expressed by Equation (3). Substituting Equations (3) and (11)–(15) into Equation (10), fluid-induced forces (F_x and F_y) are obtained by nonlinear dynamic model. They are compared with the forces from transient CFD simulations, as shown in Figures 20 and 21
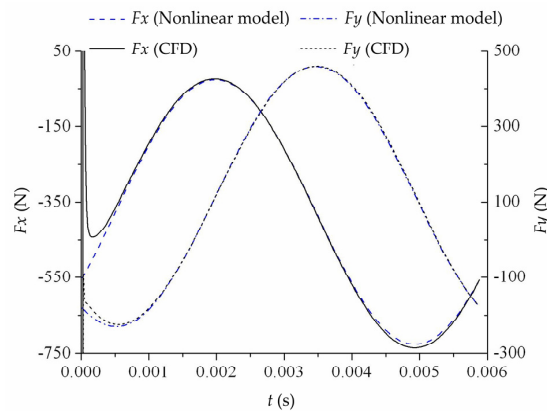

Figure 20. Fluid forces induced by the circular whirl around seal center (se/C_r 20%).
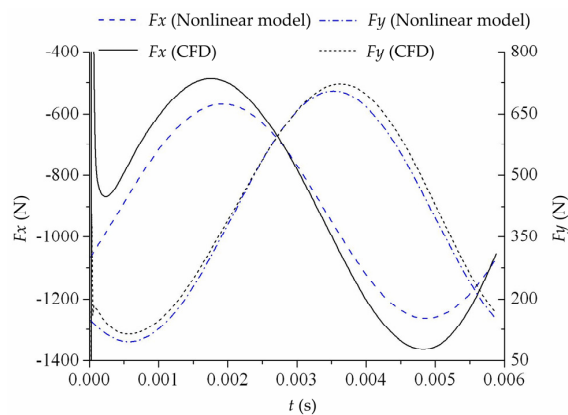

Figure 21. Fluid forces induced by the circular whirl around seal center (se/C_r 50%).

As shown in Figure 20, for the circular whirl around the static position with eccentricity ratio 20%, fluid forces from nonlinear dynamic model and transient CFD simulations agree well.

Maximum differences are 9.42 N for F_x and 4.65 N for F_y. However, when the static eccentricity ratio increases to 50%, fluid force curves obtained by these two approaches are no longer consistent, as shown in Figure 21. The maximum differences are 111 N for F_x and 36.7 N for F_y. This indicates that the nonlinear dynamic model has low reliability for rotor disturbances under large eccentricity. However, the circular whirl around concentric position is an exception (see Figure 19). The nonlinear dynamic model can deal with it well. The two rotor motions corresponding to Figures 19 and 21 are both under large eccentricities. The only difference is their motion ways. The rotor motion corresponding to Figure 19 is the whirl around seal center, and "nominal" force coefficients used for generating the nonlinear dynamic model are based on this motion way. Therefore, it is understandable that the nonlinear model applies well. From this point of view, the reason that nonlinear dynamic model does not suitable for circular whirls around large eccentricity position (as shown in Figure 21) can be assumed to be that the force coefficients (or dynamic characteristics) of annular seal under large eccentricity are related to rotor motion ways.

4.3. 1D Harmonic Shaking Motions

To validate the assumption proposed above, the circular whirl around the static position with eccentricity ratio 50% is divided into two separate 1D shaking motions, as shown in Figure 22. One is the shaking motion in X direction; the other is in Y direction. The Y direction is also the tangential direction of the concentric whirl. Namely, the Y-directional shaking is somewhat similar to the circular whirl around seal center. The expressions of two shaking motions are, respectively, presented in Equations (17) and (18). The amplitude A is 10% C_r and the harmonic frequency Ω corresponds to the speed 10,200 r/min.

$$\begin{cases} x = se + A\cos(\Omega t) \\ \quad y = 0 \end{cases} \tag{17}$$

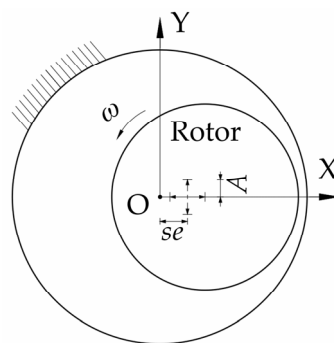$$\begin{cases} \quad x = se \\ y = A\sin(\Omega t) \end{cases} \tag{18}$$

Figure 22. Two harmonic shaking motions.

According to motion equations of two harmonic shakings, fluid-induced forces can be obtained by nonlinear dynamic model and transient CFD simulations. They are shown in Figures 23 and 24. The comparison with transient CFD simulations shows that the reliability of nonlinear dynamic model is low in predicting fluid forces induced by X-directional shaking. Maximum differences of two approaches are 119 N for F_x and 30.8 N for F_y. However, as to the Y-directional shaking, the reliability of the nonlinear model is obviously improved, as shown in Figure 24. This can be attributed to the slight likeness of Y-directional shaking with the circular whirl around seal center. In Figure 20, maximum differences of two approaches are 18.5 N for F_x and 17.7 N for F_y, and they are much smaller than those in Figure 23. Namely, the nonlinear dynamic model is more applicable to rotor disturbances similar to the circular whirl around concentric position. The assumption proposed in Section 4.2 is confirmed and can explain the low reliability of nonlinear dynamic model. Under large eccentricity, the dynamic

characteristics of seals are varied with the motion ways of the rotor, and the nonlinear dynamic model based on a specific motion way is incompetent in dealing with all kinds of rotor disturbances.
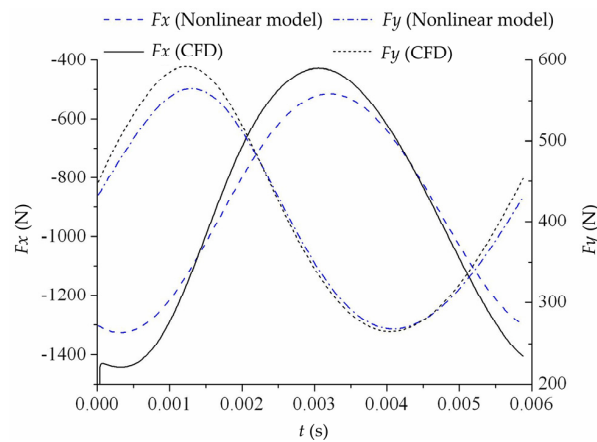

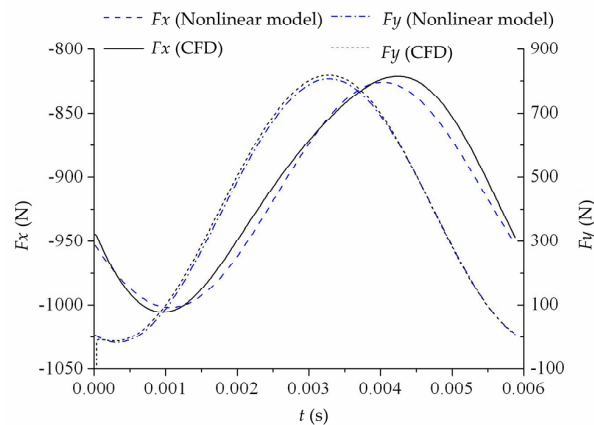**Figure 23.** Fluid forces induced by X-directional shaking.

Figure 24. Fluid forces induced by Y-directional shaking.

4.4. Quasi-Circular (Spiral) Whirl

In this section, the rotor is assumed to perform the circular whirl around seal center with growing whirl radius, i.e., the spiral whirl, in order to validate the suitability of nonlinear dynamic model for quasi-circular whirls no matter eccentricity magnitudes. The whirling speed is r/min and the rotor eccentricity ratio rises linearly to 60% within six whirl periods. The whirl equation is presented in Equation (17) and the whirl orbit is shown in Figure 25.

$$\begin{cases} x = f \cdot t cos(\Omega t) \\ y = f \cdot t sin(\Omega t) \end{cases}, \tag{19}$$

where *T* is the whirl period and $f = 60\% \, C_r/(6 \, T)$, indicating the eccentricity speed of the rotor.

In actual applications, the spiral whirl in Figure 25 represents the destabilizing process of the rotor. Fluid forces induced by the destabilizing whirl are obtained, respectively, by nonlinear dynamic model and transient CFD simulations. They are shown in Figure 26. The rise of rotor eccentricity with time leads to the increasing fluid force (i.e., the resultant force of F_x and F_y). The F_x and F_y from nonlinear model are in good agreement with those from transient CFD simulations. Maximum differences of two approaches are 42.7 N (i.e., relative error 2.3%) for F_x and 35.7 N (relative error 2.3%) for F_y. Namely, nonlinear dynamic model is reliable in evaluating fluid forces induced by the quasi-circular whirl around seal center without special limitations on eccentricity magnitudes.
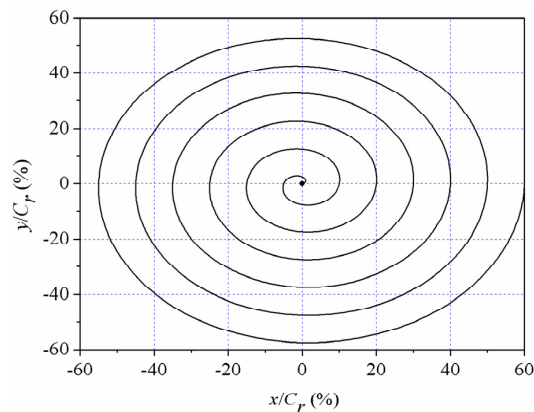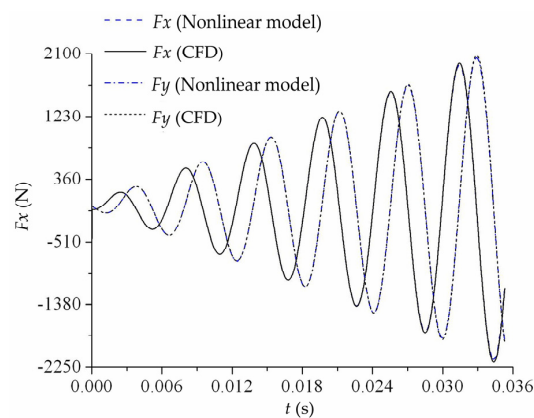
Figure 25. Spiral whirl orbit of the rotor.

Figure 26. Fluid forces induced by the spiral whirl around seal center.

5. Conclusions

In the paper, dynamic characteristics of the annular plain liquid seal under various large rotor disturbance motions are studied using the transient CFD method based on dynamic mesh technique and nonlinear Muszynska' model.

Force coefficients and leakage rates of annular seal under different static eccentricities are evaluated. The reliability of transient CFD simulation is validated by comparing the force coefficients and leakage rates with those from the Marquette's experiment and bulk flow method. With increasing static eccentricity, these force coefficients show clearly asymmetric behavior and obvious changes. The force coefficients from transient CFD simulations show a high consistency with experimental values despite the different values of stiffness. The error sources are mainly form the influence of upstream and inlet boundary condition due to the drawback of the experimental apparatus for absent inlet control. Leakage rates computed by the CFD method fit better to measured values than those from the bulk flow method, which indicates that leakage rates are insensitive to static eccentricity.

As to the concentric annular seal, its dynamic characteristics are usually supposed to be linear (namely, constant force coefficients) when the rotor disturbance is within 10% C_r. However, this conclusion is not suitable for the eccentric annular seal, especially the seal under large static eccentricity. As rotor static eccentricity increases, the force characteristics of annular seal become more sensitive to whirl amplitude, in other words, the linear range of dynamic characteristics narrows gradually. With respect to the concentric seal, the annular seal with large eccentricity is easier to show nonlinear characteristics.

According to the Muszynska's model, a nonlinear dynamic model is presented in the paper for describing nonlinear seal forces induced by rotor large disturbances. The suitability of the nonlinear model for all kinds of rotor disturbances is studied through four forms of rotor motions.

The nonlinear dynamic model is suitable for various rotor disturbances when the rotor is under small static eccentricity (e.g., eccentricity ratio under 20%). However, when rotor static eccentricity is large (e.g., eccentricity ratio 50%), the nonlinear dynamic model based on circular whirls around eccentric center becomes incompetent and unsatisfactory. It shows high reliability only for circular or quasi-circular whirls around concentric center. This means that dynamic characteristics of annular seal under large disturbance are related to rotor motion ways. For the annular seals under large dynamic eccentricity (whirl amplitude) and rather small static eccentricity (e.g., static eccentricity ratio under 20% in this case), the nonlinear Muszynska's model performs well when dealing with large rotor disturbances. The range of capability of this nonlinear model depends on the typical parameters of annular seals. It can also explain why Muszynska's model is out of action when rotor–seal system has a large eccentricity ratio in He's research.

On the whole, dynamic characteristics of annular seals under large disturbance are very complex. They are very sensitive to various rotor motion ways including whirl amplitude and static eccentricity. For the seal with large disturbances motion of a small static eccentricity, the nonlinear Muszynska's model performs reliably, which provides a solid basis for the seal–rotor system analysis using nonlinear seal force model. The capability and limitation of nonlinear dynamic model under large disturbances needs further investigation.

Author Contributions: Conceptualization, K.Z. and D.W.; methodology, K.Z., X.J. and P.W.; validation, D.W. and P.W.; formal analysis, K.Z. and X.J.; investigation, K.Z., S.L. and P.W.; resources, D.W.; data curation, K.Z., X.J. and S.Y.; writing—original draft preparation, K.Z. and X.J.; writing—review and editing, S.L. and S.Y.; visualization, K.Z.; supervision, P.W. and D.W.; project administration, B.H. and D.W.; and funding acquisition, B.H. All authors have read and agreed to the published version of the manuscript.

Nomenclature

$C: c$	Direct and cross damping coefficients of concentric annular seal (N·s/m)
$c_{xx}, c_{yy}, c_{xy}, c_{yx}$	Damping coefficients of eccentric annular seal (N·s/m)
C_r	Seal clearance (mm)
e	Rotor eccentricity or whirl radius (mm]
f	Eccentricity speed of the rotor
F_x, F_y	Fluid forces in X and Y directions (N)
F_{x0}, F_{y0}	Fluid forces at equilibrium position (N)
$\Delta F_x, \Delta F_y$	The increments of fluid forces relative to F_{x0} and F_{y0} (N)
K, k	Direct and cross stiffness coefficients of concentric seal (N/m)
$k_{xx}, k_{yy}, k_{xy}, k_{yx}$	Stiffness coefficients of eccentric annular seal (N/m)
M	Direct mass coefficient of concentric annular seal (kg)
m_{xx}, m_{yy}	Direct mass coefficients of eccentric annular seal (kg)
ra	Ratio of the distance between the nodes in the clearance domain and the outer static wall to the clearance
se	Rotor static eccentricity (mm)
se/C_r	Static eccentricity ratio
t	Time (s)
x, y	The displacements of rotor center (mm)
$\Delta x, \Delta y$	Rotor displacements relative to equilibrium position (mm)
Δe	Rotor dynamic eccentricity (mm)
ε	Eccentricity ratio (e/C_r)
ω	Rotating speed of the rotor (rpm)
Ω	Whirling speed of the rotor (rpm)

References

1. Du, Q.; Zhang, D. Numerical investigation on flow characteristics and aerodynamic performance of a 1.5-stage SCO2 axial-inflow turbine with labyrinth seals. *Appl. Sci.* **2020**, *10*, 373. [CrossRef]
2. Wang, X.; Liu, M.; Kao-Walter, S.; Hu, X. Numerical Evaluation of Rotordynamic Coefficients for Compliant Foil Gas Seal. *Appl. Sci.* **2020**, *10*, 3828. [CrossRef]
3. Xia, P.; Chen, H.; Liu, Z.; Ma, W.; Yang, B. Analysis of Whirling Motion for the dynamic System of Floating Ring Seal and Rotor. *Proc. Inst. Mech. Eng. Part J J. Eng. Tribol.* **2019**, *233*, 1–15. [CrossRef]
4. Awad, H.; Parrondo, J.; González, V. Vibrations in Leaking Spherical Valves with Annular Seal. *Proceedings* **2018**, *2*, 1444. [CrossRef]
5. Zhai, L.; Wu, G.; Wei, X.; Qin, D.; Wang, L. Theoretical and Experimental Analysis for Leakage Rate and Dynamic Characteristics of Herringbone-Grooved Liquid Seals. *Proc. Inst. Mech. Eng. Part J J. Eng. Tribol.* **2015**, *229*, 849–860. [CrossRef]
6. Ikemoto, A.; Inoue, T.; Sakamoto, K.; Uchiumi, M. Nonlinear Analysis of Rotordynamic Fluid Forces in the Annular Plain Seal by Using Extended Perturbation Analysis of the Bulk-Flow Theory (Influence of Whirling Amplitude in the Case with Concentric Circular Whirl). *J. Tribol.* **2018**, *140*, 1–15. [CrossRef]
7. Gao, R.; Kirk, G. CFD Study on Stepped and Drum Balance Labyrinth Seal. *Tribol. Trans.* **2013**, *56*, 663–671. [CrossRef]
8. Untaroiu, A.; Hayrapetian, V.; Untaroiu, C.D.; Wood, H.G.; Schiavello, B.; McGuire, J. On the Dynamic Properties of Pump Liquid Seals. *J. Fluids Eng.* **2013**, *135*, 051104. [CrossRef]
9. Li, F.; Cui, B.; Zhai, L. Research on Rotordynamic Characteristics of Pump Annular Seals Based on a New Transient CFD Method. *Processes* **2020**, *8*, 227. [CrossRef]
10. Childs, D.W.; Arthur, S.P. Static Destabilizing Behavior for Gas Annular Seals at High Eccentricity Ratios. In Proceedings of the ASME Turbo Expo 2013: Turbine Technical Conference and Exposition, San Antonio, TX, USA, 3–7 June 2013; Volume 7A, pp. 1–7.
11. Nelson, C.C.; Nguyen, D.T. Analysis of Eccentric Annular Incompressible Seals: Part 1—A New Solution Using Fast Fourier Transforms for Determining Hydrodynamic Force. *J. Tribol.* **1988**, *110*, 354. [CrossRef]
12. Andres, L.A.S. Analysis of Variable Fluid Properties, Turbulent Annular Seals. *J. Tribol.* **1991**, *113*, 694–702. [CrossRef]
13. Arghir, M.; Frene, J. A Bulk-Flow Analysis of Static and Dynamic Characteristics of Eccentric Circumferentially-Grooved Liquid Annular Seals. *J. Tribol.* **2004**, *126*, 316–325. [CrossRef]
14. Venkataraman, B.; Palazzolo, A.B. Thermohydrodynamic Analysis of Eccentric Annular Seals Using Cubic Spline Interpolations©. *Tribol. Trans.* **1997**, *40*, 183–194. [CrossRef]
15. Athavale, M.M.; Hendricks, R.C. A Small Perturbation CFD Method for Calculation of Seal Rotordynamic Coefficients. *Int. J. Rotating Mach.* **1996**, *2*, 167–177. [CrossRef]
16. Wu, D.; Jiang, X.; Li, S.; Wang, L. A New Transient CFD Method for Determining the Dynamic Coefficients of Liquid Annular Seals. *J. Mech. Sci. Technol.* **2016**, *30*, 3477–3486. [CrossRef]
17. Andres, L.S.; Jeung, S.H. Orbit-Model Force Coefficients for Fluid Film Bearings: A Step beyond Linearization. *J. Eng. Gas Turbines Power* **2016**, *138*, 1–11.
18. Muszynska, A.; Bently, D.E. Frequency-swept Rotating Input Perturbation Techniques and Identification of the Fluid Force Models in Rotor/Bearing/Seal Systems and Fluid Handling Machines. *J. Sound Vib.* **1990**, *143*, 103–124. [CrossRef]
19. Li, Z.G.; Chen, Y.S. Research on 1:2 Subharmonic Resonance and Bifurcation of Nonlinear Rotor-Seal System. *Appl. Math. Mech. (English Ed.)* **2012**, *33*, 499–510. [CrossRef]
20. He, H.J.; Jing, J.P. Research into the Dynamic Coefficient of the Rotor-Seal System for Teeth-on-Stator and Teeth-on-Rotor Based on an Improved Nonlinear Seal Force Model. *J. Vib. Control* **2014**, *20*, 2288–2299. [CrossRef]
21. Marquette, O.R.; Childs, D.W.; San Andres, L. Eccentricity Effects on the Rotordynamic Coefficients of Plain Annular Seals: Theory Versus Experiment. *J. Tribol.* **1997**, *119*, 443. [CrossRef]
22. Childs, D.W.; Arthur, S.; Mehta, N.J. The Impact of Hole Depth on the Rotordynamic and Leakage Characteristics of Hole-Pattern-Stator Gas Annular Seals. *J. Eng. Gas Turbines Power* **2013**, *136*, 042501. [CrossRef]

23. Muszynska, A. Whirl and Whip—Rotor/Bearing Stability Problems. *J. Sound Vib.* **1986**, *110*, 443–462. [CrossRef]
24. Muszynska, A. Improvements in Lightly Loaded Rotor/Bearing and Rotor/Seal Models. *J. Vib. Acoust. Stress. Reliab. Des.* **1988**, *110*, 129–136. [CrossRef]
25. Li, Q.; Liu, S.; Pan, X.; Zheng, S. A New Method for Studying the 3D Transient Flow of Misaligned Journal Bearings in Flexible Rotor-Bearing Systems. *J. Zhejiang Univ. Sci. A* **2012**, *13*, 293–310. [CrossRef]
26. Childs, D.W. Dynamic Analysis of Turbulent Annular Seals Based On Hirs' Lubrication Equation. *J. Lubr. Technol.* **1983**, *105*, 429–436. [CrossRef]
27. Ha, T.W.; Choe, B.S. Numerical Simulation of Rotordynamic Coefficients for Eccentric Annular-Type-Plain-Pump Seal Using CFD Analysis. *J. Mech. Sci. Technol.* **2012**, *26*, 1043–1048. [CrossRef]
28. Wu, D.; Jiang, X.K.; Chu, N.; Wu, P.; Wang, L.Q. Numerical Simulation on Rotordynamic Characteristics of Annular Seal under Uniform and Non-Uniform Flows. *J. Cent. South Univ.* **2017**, *24*, 1889–1897. [CrossRef]
29. Yan, X.; Li, J.; Feng, Z. Investigations on the Rotordynamic Characteristics of a Hole-Pattern Seal Using Transient CFD and Periodic Circular Orbit Model. *J. Vib. Acoust.* **2011**, *133*, 041007. [CrossRef]